Peripapillary RNFL Imaging

Jin Wook Jeoung

Abstract

Glaucoma is an optic neuropathy characterized by progressive loss of retinal ganglion cells and their axons. Detection of glaucoma is based on the identification of abnormalities in the optic nerve head or the retinal nerve fiber layer (RNFL), either structural or functional. Several techniques including clinical examination, red-free fundus photography, and modern imaging devices are currently available for detecting and quantifying RNFL damage. Optical coherence tomography (OCT) is one of the most recent technologies allowing for quantitative assessment of the peripapillary RNFL. Several studies investigating the performance of OCT in glaucoma have shown promising results. However, as with other technologies, imaging may produce false identification of glaucoma; thus, clinicians should not depend solely on the results of one single imaging device. Recent studies also suggest that glaucoma imaging devices may serve as a useful adjunct in accurately and objectively assessing the degree of glaucomatous damage. Peripapillary RNFL imaging by OCT technology can provide useful measures that assist the clinician in the early detection of glaucoma. This chapter details OCT-based peripapillary RNFL imaging used for diagnosis of glaucoma and monitoring of disease progression.

Keywords

Glaucoma · Optical coherence tomography
Retinal nerve fiber layer

1 Introduction

Glaucoma is an optic neuropathy characterized by structural changes to the optic nerve head and retinal nerve fiber layer (RNFL), with corresponding visual field loss. RNFL loss is thought to precede measurable optic nerve head and visual field damage (Sommer et al. 1977, 1991). Thus, evaluation of peripapillary RNFL damage is an important method for detecting glaucomatous changes, particularly early in the glaucoma continuum.

Several techniques including clinical examination, red-free fundus photography, and modern imaging devices are available for detecting and quantifying RNFL damage. Optical coherence tomography (OCT) is one of the most recent technologies allowing for quantitative assessment of RNFL thickness. Moreover, OCT's diagnostic

J. W. Jeoung (✉)
Department of Ophthalmology, Seoul National University Hospital, Seoul National University College of Medicine, Jongno-gu, Seoul, Korea
e-mail: jwjung76@snu.ac.kr

© The Author(s), under exclusive license to Springer Nature Singapore Pte Ltd. 2021

K. H. Park, T.-W. Kim (eds.), *OCT Imaging in Glaucoma*,
https://doi.org/10.1007/978-981-16-1178-0_2

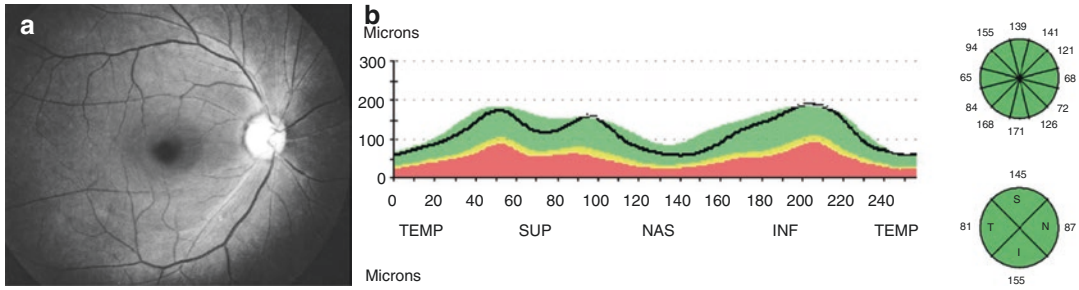

Fig. 1 RNFL images of a normal healthy eye. (**a**) Red-free RNFL photography. (**b**) OCT TSNIT (temporal–superior–nasal–inferior–temporal) RNFL thickness graph and OCT sector (clock-hour and quadrant) plots

classifications based on its internal normative database enables clinicians to assess structural glaucomatous damage more efficiently.

Recently, there has been considerable improvement in OCT technology. Spectral-domain OCT (SD-OCT), for example, offers several advantages over time-domain OCT (TD-OCT). With its faster scan speed, it allows for the acquisition of OCT data with fewer motion artifacts. Another advantage of SD-OCT over TD-OCT is the improved axial resolution (5–8 μm (SD-OCT) vs. 8–10 μm (TD-OCT) in tissue).

2 Histology and Anatomy of Retinal Nerve Fiber Layer (RNFL)

The RNFL contains the retinal ganglion cell axons covered by astrocytes and bundled by the Müller cell processes. The retinal nerve fibers are ophthalmoscopically detectable as bright and fine striations in the inner retinal layer (Hoyt et al. 1973; Airaksinen et al. 1984; Airaksinen and Nieminen 1985). According to an electron microscopic study, these fine striations appear to be bundles of axons compartmentalized within glial tunnels formed by the Müller cell processes (Radius and Anderson 1979).

The RNFL is distributed in a characteristic pattern. Axons arising from the temporal retina arc, above or below the macula, enter the superior temporal and inferior temporal areas, respectively, of the optic nerve head in an arcuate pattern. Those arising in the macular region pass directly to the temporal edge of the optic nerve, forming the papillomacular bundle.

Dividing the fundus into eight regions, the nerve fiber bundles are most visible in the temporal inferior region, followed by the temporal superior region, the nasal superior region, and finally the nasal inferior region (Jonas et al. 1989). It is least visible in the superior, inferior, temporal horizontal, and nasal horizontal regions. Figure 1 shows the RNFL images of a normal healthy eye.

3 Clinical Findings on Peripapillary RNFL in Glaucoma

Since Hoyt et al. (1973) initially described RNFL atrophy in glaucoma, evaluation of the RNFL has been essential to glaucomatous optic neuropathy diagnostics. For detection and quantification of RNFL damage, several techniques including red-free RNFL photography and modern imaging devices have been proposed. Clinically, RNFL atrophy can be divided into localized atrophy (wedge-shaped defect) and diffuse atrophy. The localized defects are not spindle-like defects but wedge-shaped ones that run toward or touch the optic disc border (Jonas and Dichtl 1996).

4 OCT Reproducibility for Peripapillary RNFL Measurements

OCT RNFL thickness measurements have been shown to be reproducible and reliable. Several studies evaluated the reproducibility of OCT RNFL thickness measurements from various SD-OCT devices. Leung et al. (2009) reported

that the intravisit repeatability of Cirrus HD-OCT ranged between 5.12 and 15.02 μm, and the intervisit reproducibility ranged between 4.31 and 22.01 μm. Vizzeri et al. (2009) and González-García et al. (2009) showed excellent reproducibility levels that can be obtained by different SD devices (Cirrus and RTVue OCT). Vizzeri et al. (2009) showed that the coefficient of variation and intra-class correlation for average RNFL thickness were 1.5% and 0.96, respectively, in healthy eyes and 1.6% and 0.98, respectively, in glaucomatous eyes.

5 Glaucoma Diagnostic Performance of SD-OCT

Several studies investigating the performance of OCT in glaucoma have shown promising results. Earlier studies reported that RNFL thickness in the inferior region often had the best ability to discriminate normal eyes from eyes with early to moderate glaucoma, with sensitivities between 64% and 79% for specificities of 90% or higher (Bowd et al. 2001; Kanamori et al. 2003; Medeiros et al. 2004). Also, several studies have investigated the diagnostic capability of SD-OCT RNFL thickness measurements using an area-under-the-receiver-operating-characteristic curve (AUROC) for discrimination between healthy and glaucomatous eyes, which have shown that the AUROCs of the RNFL parameter ranged from 0.60 to 0.98, depending on the parameters and the characteristics of the population evaluated (Leite et al. 2010, 2011; Mwanza et al. 2012; Jeoung et al. 2013).

6 Diagnostic Accuracy in Preperimetric Glaucoma

In the study from Korea that enrolled 55 preperimetric glaucoma patients and 55 age- and sex-matched controls, the sensitivity of the Cirrus OCT parameters ranged from 21.0% to 87.1% with the criterion of abnormal at the 5% level (Jeoung and Park 2010). Based on the normative database, the highest Cirrus OCT sensitivity was obtained with the deviation-from-normal map (sensitivity 87.1% and specificity 61.8%). Another study by Jeoung et al. (2014) evaluated the diagnostic abilities of the speckle noise-reduced spectral-domain optical coherence tomography (SD-OCT; Spectralis OCT) and time-domain optical coherence tomography (TD-OCT; Stratus OCT) to detect localized retinal nerve fiber layer (RNFL) defects in patients with preperimetric open-angle glaucoma. They found that the AUROC for the best parameter from SD-OCT (inferotemporal sector, AUROC = 0.940) was significantly higher than that of TD-OCT (7 o'clock sector, AUROC = 0.881; P = 0.009), suggesting that speckle noise-reduced SD-OCT is better able to detect preperimetric localized RNFL defects than TD-OCT.

7 Instrument-Specific Maps and Interpretation

7.1 Cirrus HD-OCT

Cirrus OCT extracts from the data cube 256 A-scan samples along the path of the calculation circle. Based on the RNFL layer boundaries in the extracted circle scan image, the Cirrus OCT calculates the RNFL thickness at each point along the circle. Using these data, Cirrus OCT provides the 12-clock-hour thicknesses, 4-quadrant thicknesses, a global 360° average thickness, and TSNIT (temporal–superior–nasal–inferior–temporal) thickness profiles. For each parameter, the Cirrus OCT software provides a classification (within normal limits, borderline, or outside normal limits) based on comparison with an internal normative database.

The Cirrus OCT has a normative database generated from 284 healthy individuals with a mean age of 46.5 years. For the Cirrus normative database, 43% were Caucasians, 24% were Asians, 18% were African American, 12% were Hispanic, 1% were Indian, and 6% were of mixed ethnicity. The individuals were age-stratified into six groups: 18–29, 30–39, 40–49, 50–59, 60–69, and 70 and older (Chong and Lee 2012).

The Cirrus OCT printout also provides deviation-from-normal maps that are derived from superpixel average thickness measurements and report a statistical comparison against the normal thickness range for each superpixel, overlaid on the OCT fundus image. These maps apply the yellow and red colors of the age-matched normative data to superpixels whose average thickness falls in the yellow and red normal distribution percentiles (i.e., 1%–5% and <1% of normal distribution percentiles, respectively). Figures 2 and 3 demonstrate the Cirrus HD-OCT RNFL analysis printouts.

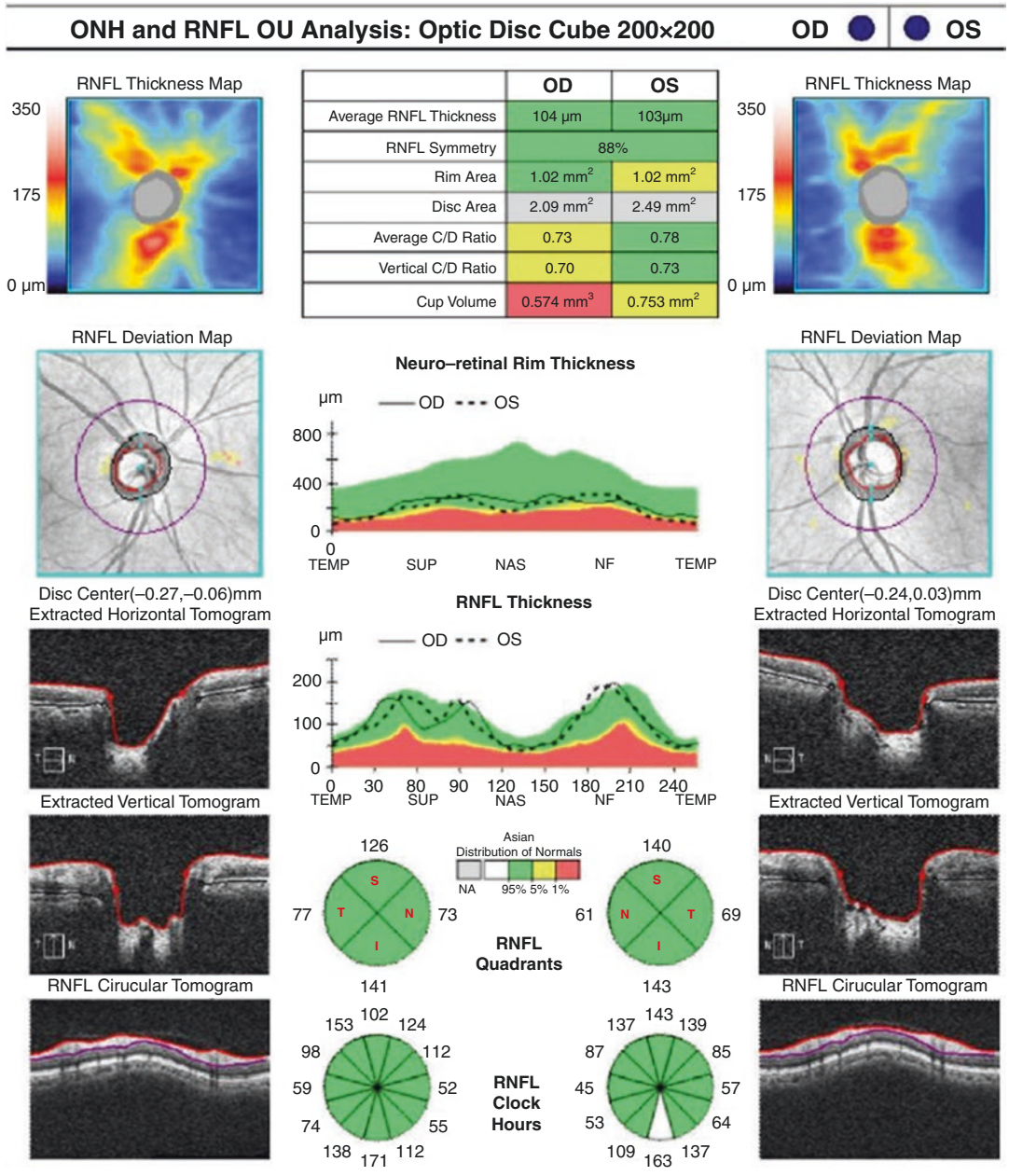

Fig. 2 Cirrus OCT retinal nerve fiber layer analysis. A case without glaucoma who has normal RNFL thickness on thickness maps, deviation maps, RNFL thickness plots, quadrant, and clock-hour plots

7.2 Spectralis OCT

The Spectralis OCT uses a superluminescent diode laser with a center wavelength of 840 nm. During OCT imaging, a scan circle with a diameter of approximately 3.46 mm was manually positioned at the center of the optic disc while the eye-tracking system was activated. This instrument combines confocal laser scanning ophthalmoscopy, which enables real-time three-dimensional tracking of eye movements, with real-time averaging of multiple B-scans acquired at an identical location of interest on the retina, to reduce speckle noise (Hangai et al. 2009). RNFL boundaries were automatically delineated according to software algorithms underneath the circumpapillary circle. The RNFL in each image was then automatically segmented. These values were averaged to yield a global average and sectoral (temporal, superotemporal, superonasal, nasal, inferonasal, and inferotemporal sectors) RNFL thickness measurement. Figure 4 shows a representative case of bilateral glaucoma with two different OCT printouts (Cirrus and Spectralis OCT).

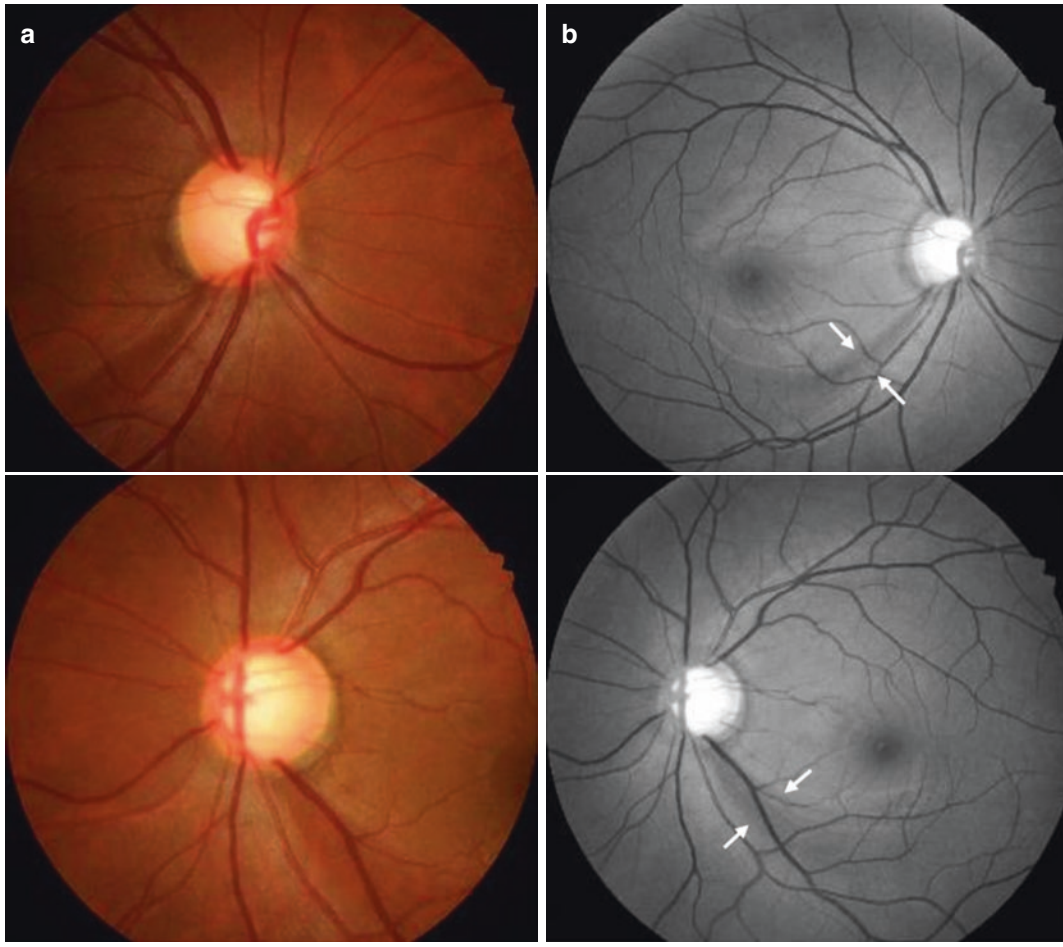

Fig. 3 Glaucoma Patient 1. (**a**, **b**) Optic disc photography and red-free RNFL photography show inferotemporal RNFL defects on both eyes. (**c**) The Cirrus OCT printout shows thinning of the RNFL in the inferotemporal region of both eyes

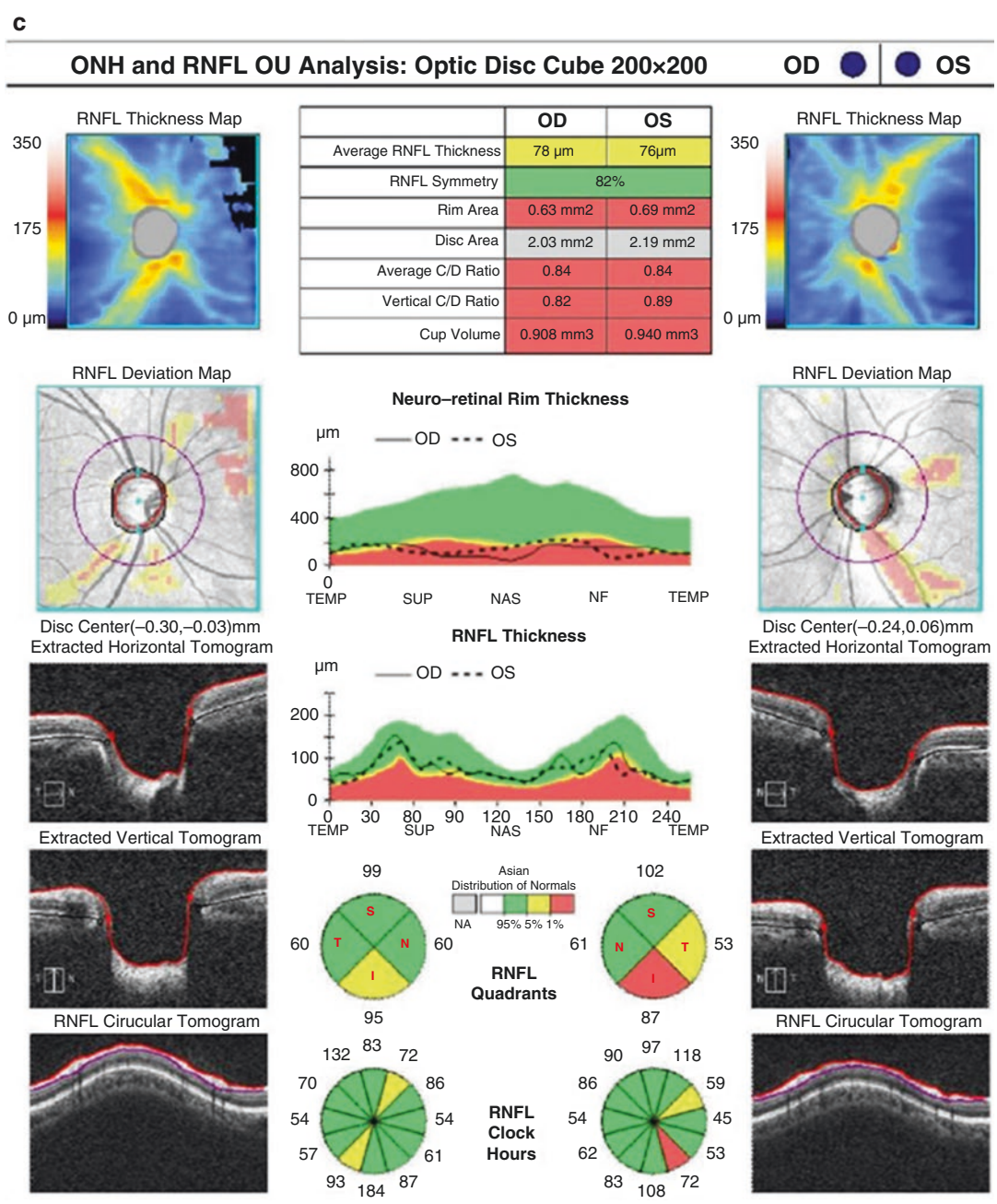

Fig. 3 (continued)

7.3 Topcon DRI-OCT

The DRI-OCT is an SS-OCT device that uses a wavelength-sweeping laser with a center wavelength of 1050 nm and a tuning range of 100 nm. In total, 100,000 A-scans with a 5 µm axial resolution in tissue are acquired per second. The DRI-OCT can provide a wide-field scan protocol (12 × 9 mm), which enables to obtain images of the macular and optic nerve head region in a single scan.

With the built-in analysis software, the RNFL boundary was automatically segmented and the RNFL thickness throughout the scan was calculated. The RNFL thickness map was generated within the 12 × 9 mm wide-field area with color scales that corresponded with numeric RNFL

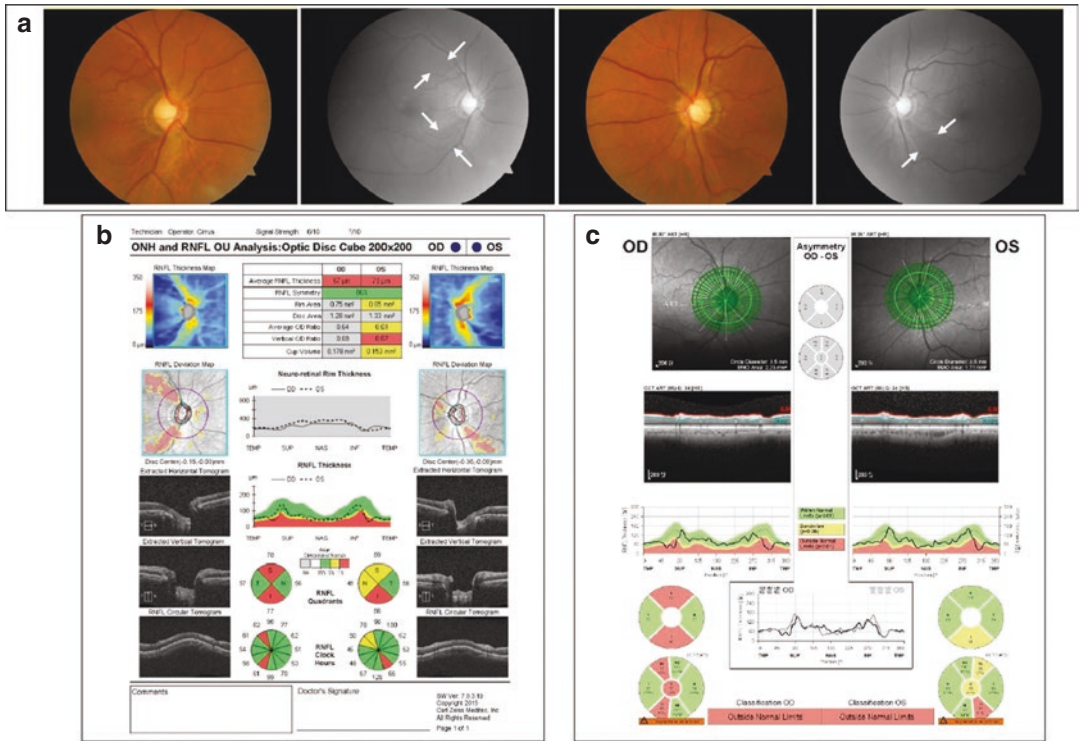

Fig. 4 Glaucoma Patient 2. (**a**) Optic disc photography and red-free RNFL photography show superotemporal and inferotemporal RNFL defects of the right eye and inferotemporal RNFL defect of the left eye. (**b**) Cirrus OCT RNFL analysis printout. (**c**) Spectralis OCT RNFL analysis printout

thickness measurements. Abnormal results based on a comparison of the RNFL and macular (GC-IPL + RNFL) thickness to the normative database are displayed on the SuperPixel deviation map. The uncolored pixels indicated the normal range, whereas the yellow- or red-colored pixels indicated abnormality at 1%–5% and <1% of the normal level, respectively. Figures 5 and 6 demonstrate the Topcon DRI-OCT maps.

8 Clinical Application of Peripapillary RNFL Imaging in Glaucoma

OCT RNFL thickness measurements are usually lower in glaucoma eyes than those in normal healthy eyes. It is well recognized that glaucomatous RNFL defects often occur at the superotemporal or inferotemporal parapapillary region, or both (Jonas and Dichtl 1996). OCT abnormal thinning of the RNFL in the superior or inferior regions can suggest the diagnosis of glaucoma.

OCT devices usually offer diagnostic classifications based on the internal normative databases. OCT color codes can provide important clues to differentiate glaucomatous eyes from healthy eyes. At the same time, careful interpretation of abnormal color codes is required because of false-positive possibilities. Kim et al. (2015) demonstrated the overall rate of false-positive diagnostic classification by SD-OCT RNFL maps as 30.8%. Longer axial length and smaller disc area were associated with abnormal RNFL diagnostic classification. Figure 7 shows the red-color regions of the RNFL (false-positive results) in a myopic healthy eye.

9 Wide-Field Map for Detection of Glaucoma

Recently, the swept-source OCT (SS-OCT) has been introduced, which has the advantages of higher speed and higher penetration with a longer wavelength than SD-OCT (Mansouri et al. 2014).

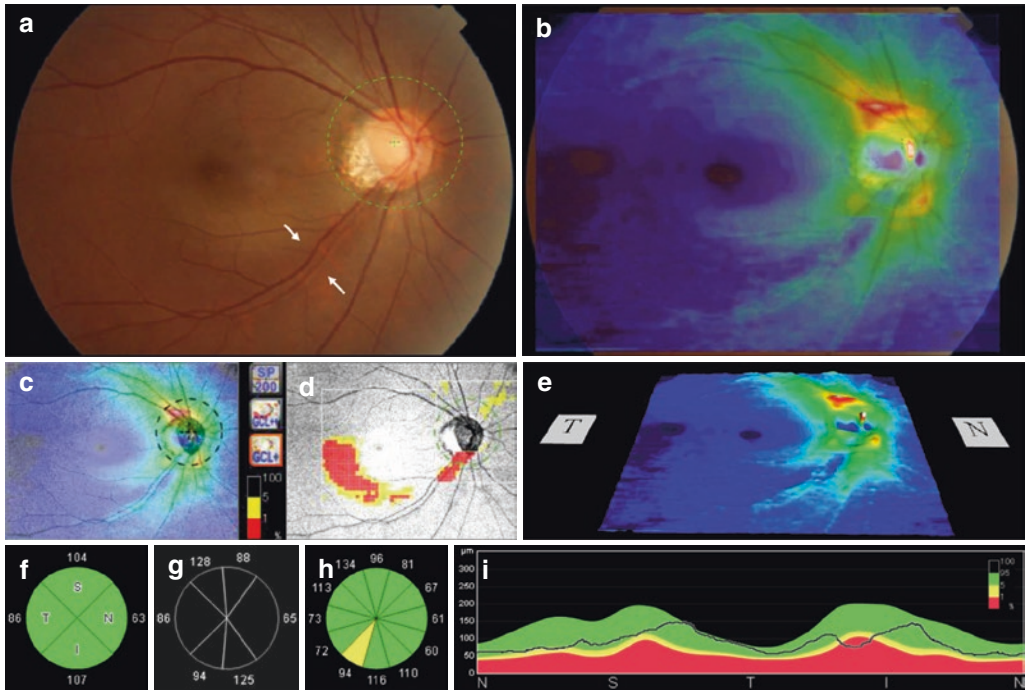

Fig. 5 Glaucoma Patient 3. Wide-field map of Topcon DRI OCT. (**a**) Fundus photography shows inferotemporal RNFL defect of the right eye. (**b**) OCT RNFL thickness map. (**c**, **d**, **e**) OCT thickness map, SuperPixel map (deviation from normal for GCIPL and RNFL thickness), and thickness surface map. (**f**, **g**, **h**, **i**) OCT Sector and RNFL thickness plots

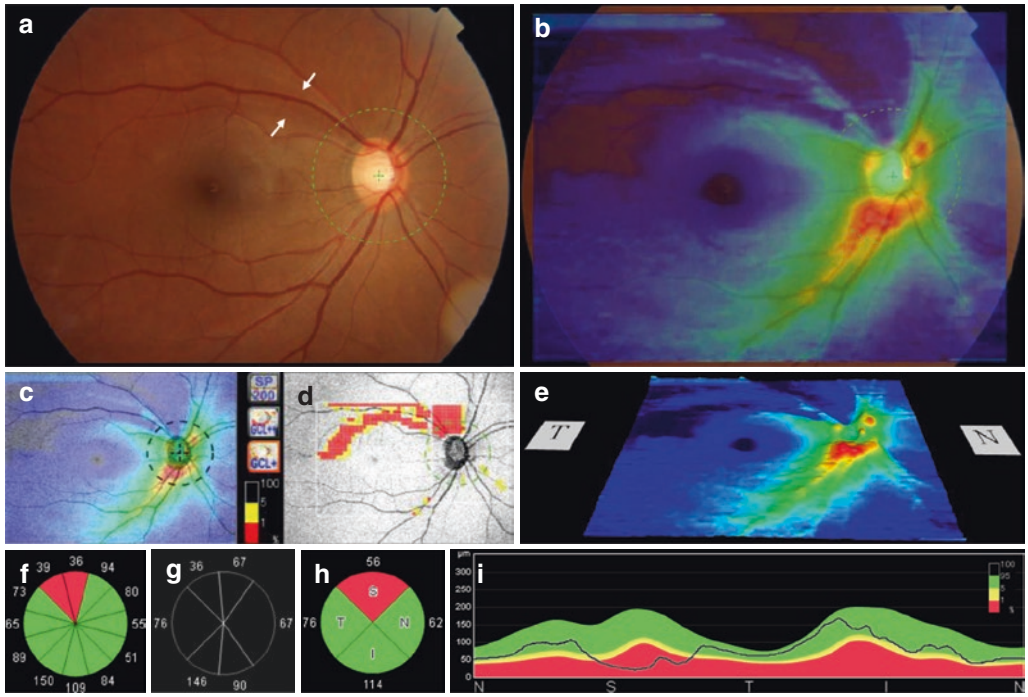

Fig. 6 Glaucoma Patient 4. Wide-field map of Topcon DRI OCT. (**a**) Fundus photography shows a superotemporal RNFL defect of the right eye. (**b**) OCT RNFL thickness map. (**c**, **d**, **e**) OCT thickness map, SuperPixel map (deviation from normal for GCIPL and RNFL thickness), and thickness surface map. (**f**, **g**, **h**, **i**) OCT Sector and RNFL thickness plots

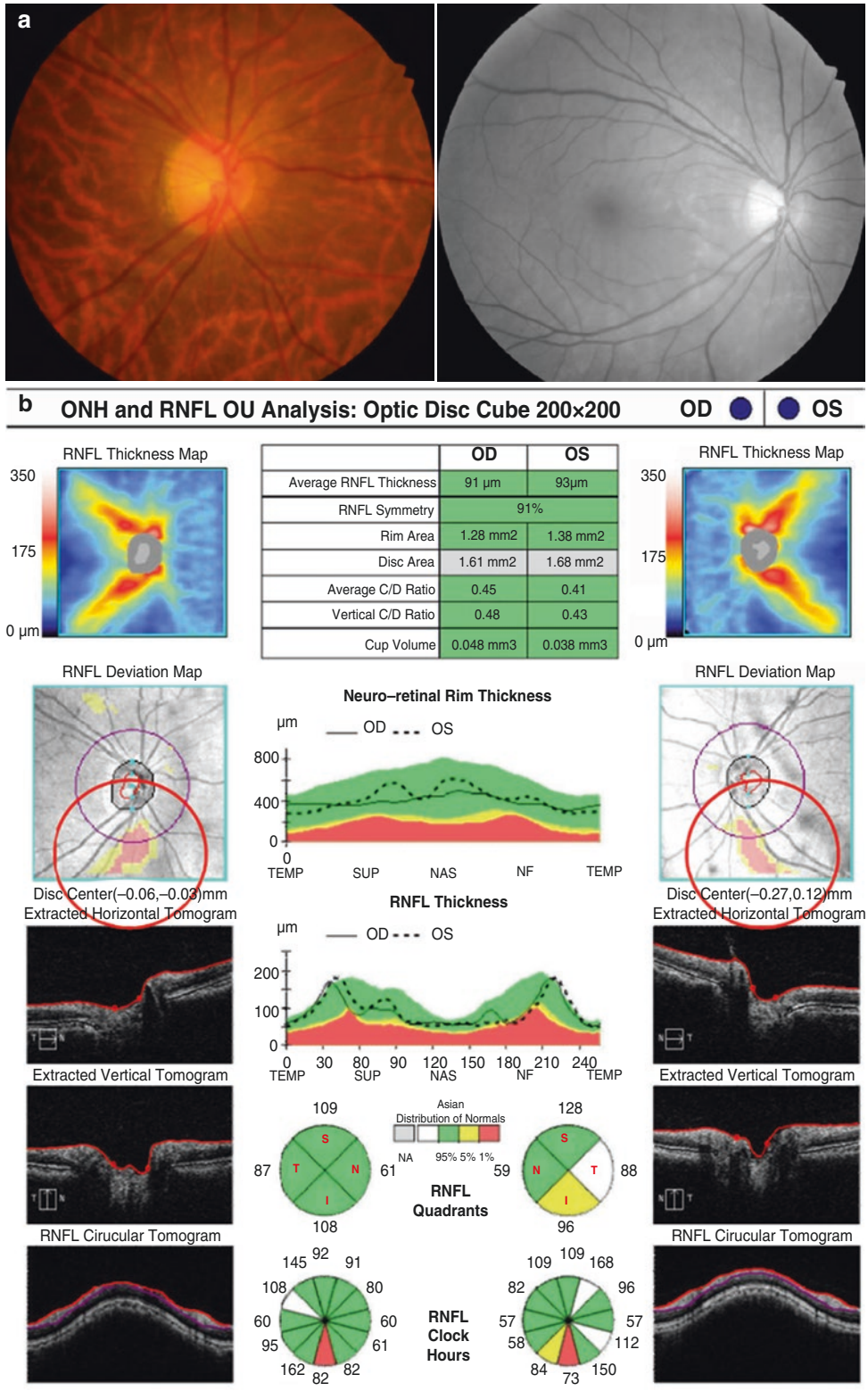

Fig. 7 A subject with the myopic healthy eye. (**a**) Optic disc photography and red-free RNFL photography. (**b**) The OCT printout shows red-color regions of the RNFL (false-positive results) in both eyes, based on the built-in normative database

Therefore, SS-OCT has been used in the glaucoma field to image deep ocular structures such as the choroid and lamina cribrosa, as well as RNFL thickness (Kim et al. 2016a, b). Also, SS-OCT can provide wide-field visualization for imaging of a larger, 12 × 9 mm area of the posterior pole including the optic nerve head and macula, with one single-scan protocol. A recent study reported that the wide-field RNFL thickness map using SS-OCT performed well in distinguishing eyes with preperimetric and early glaucoma from healthy eyes (Lee et al. 2017, 2018). The wide-field RNFL map of SS-OCT can be a useful tool for the early detection of glaucoma. Figure 8 demonstrates the clinical usefulness of wide-field maps for the detection of glaucoma.

10 Detecting Glaucoma Progression by Peripapillary RNFL Imaging

Evaluation of glaucoma progression is essential in the management of glaucoma. Recently, OCT has been widely used for detecting and monitoring structural progression in glaucoma. Assessment of progressive changes in the optic disc and RNFL is based on event analysis or trend analysis. Event-based analysis detects progression when a follow-up measurement exceeds a preestablished threshold for change from baseline. Trend-based analysis detects progression by evaluating the slope of the measured parameter over time (Bussel et al. 2014). Progression is commonly defined by trend-based analysis when a significant negative slope is detected using linear regression analysis.

Recently, commercially available software for change analysis has been introduced in OCT devices, which can provide a clinically important reference to evaluate glaucoma progression. The Guided Progression Analysis (GPA) of the Cirrus HD-OCT performs event analysis of the RNFL thickness maps and displays the area of change in the RNFL thickness change map (Fig. 9). In addition, this software reports trend and event analyses of the circumpapillary RNFL thickness profiles. Pixels exceeding the test-retest variability between a follow-up and the first and second baseline images are coded in yellow and in red if the same changes are evident on three consecutive images (Leung et al. 2012).

In Spectralis OCT, eye-tracking improves reproducibility (Langenegger et al. 2011), which in turn leads to more accurate detection of glaucoma progression. Spectralis also oversamples specific points and combines them to reduce speckle (or random noise), enhancing the visualization of structures of interest. This device provides an RNFL Change Report that includes individual baseline and follow-up scans for the overall and sectoral RNFL measurements and classifications (Abe et al. 2015). The OCT change report and trend report plot the serial exams over time to calculate the rate of change using linear regression analysis (Grewal and Tanna 2013) (Fig. 10).

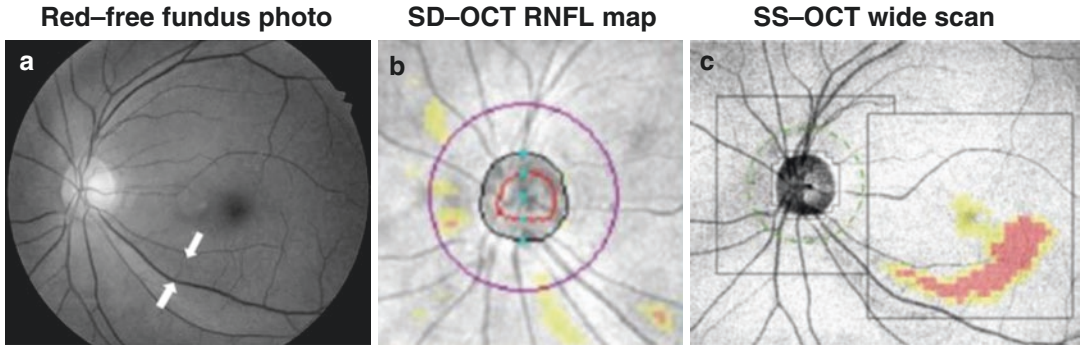

Fig. 8 A case with preperimetric glaucoma. (**a**) Conventional red-free photography revealed the inferotemporal retinal nerve fiber layer (RNFL) defect (white arrows). (**b**) SD-OCT RNFL map shows island-like isolated color patterns in the inferior and nasal areas. (**c**) The wide-field SuperPixel map (GCL+, equivalent with GCIPL in Cirrus OCT) of SS-OCT clearly showed an arcuate pattern of contiguous yellow/red abnormal pixels extending to the macular area

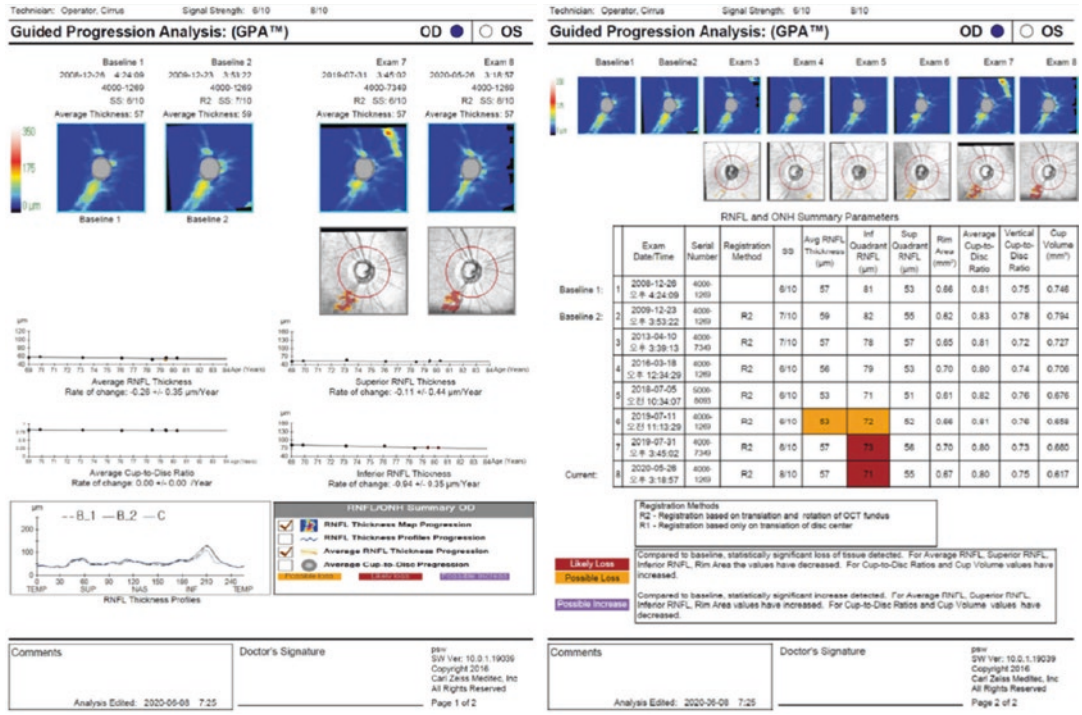

Fig. 9 Cirrus OCT guided progression analysis (GPA). Progression analysis report shows change plots over time and serial RNFL thickness maps. The OCT GPA report demonstrates the progressive RNFL thinning in the inferotemporal area

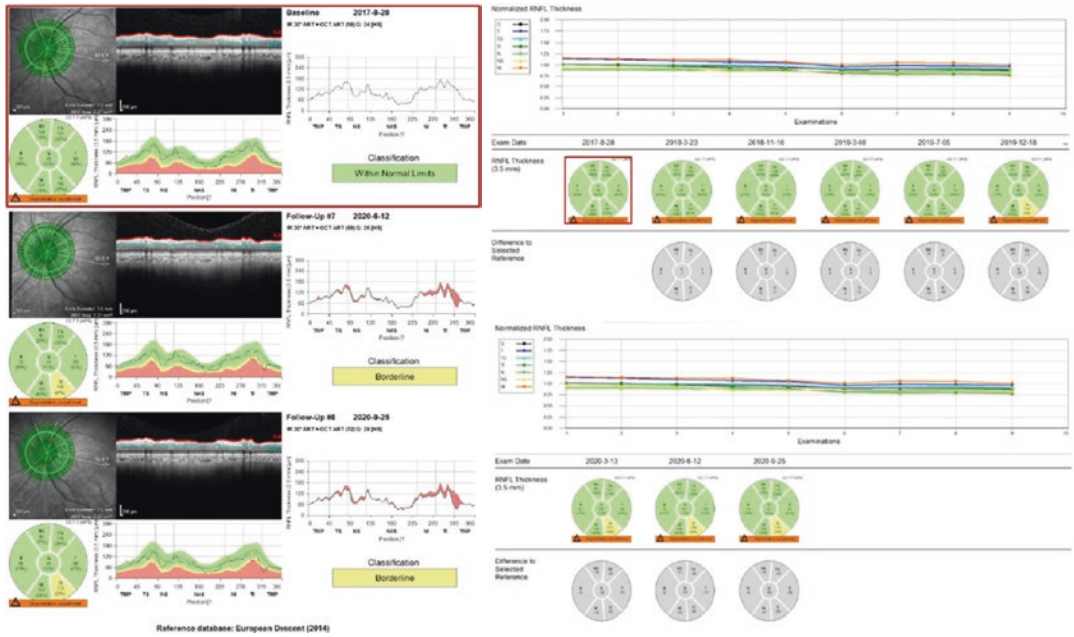

Fig. 10 Spectralis OCT scans of a glaucoma patient followed for 3 years. The RNFL change and trend reports show progressive loss of the retinal nerve fiber layer. (Courtesy of Kyeong Ik Na, M.D.)

References

Abe RY, Gracitelli CP, Medeiros FA. The use of spectral-domain optical coherence tomography to detect glaucoma progression. Open Ophthalmol J. 2015;9:78–88.

Airaksinen PJ, Nieminen H. Retinal nerve fiber layer photography in glaucoma. Ophthalmology. 1985;92(7):877–9.

Airaksinen PJ, Drance SM, Douglas GR, Mawson DK, Nieminen H. Diffuse and localized nerve fiber loss in glaucoma. Am J Ophthalmol. 1984;98(5):566–71.

Bowd C, Zangwill LM, Berry CC, Blumenthal EZ, Vasile C, Sanchez-Galeana C, et al. Detecting early glaucoma by assessment of retinal nerve fiber layer thickness and visual function. Invest Ophthalmol Vis Sci. 2001;42(9):1993–2003.

Bussel, II, Wollstein G, Schuman JS. OCT for glaucoma diagnosis, screening and detection of glaucoma progression. Br J Ophthalmol. 2014;98 Suppl 2(Suppl 2):ii15–9.

Chong GT, Lee RK. Glaucoma versus red disease: imaging and glaucoma diagnosis. Curr Opin Ophthalmol. 2012;23(2):79–88.

González-García AO, Vizzeri G, Bowd C, Medeiros FA, Zangwill LM, Weinreb RN. Reproducibility of RTVue retinal nerve fiber layer thickness and optic disc measurements and agreement with Stratus optical coherence tomography measurements. Am J Ophthalmol. 2009;147(6):1067–74, 74.e1.

Grewal DS, Tanna AP. Diagnosis of glaucoma and detection of glaucoma progression using spectral domain optical coherence tomography. Curr Opin Ophthalmol. 2013;24(2):150–61.

Hangai M, Yamamoto M, Sakamoto A, Yoshimura N. Ultrahigh-resolution versus speckle noise-reduction in spectral-domain optical coherence tomography. Opt Express. 2009;17(5):4221–35.

Hoyt WF, Frisén L, Newman NM. Fundoscopy of nerve fiber layer defects in glaucoma. Investig Ophthalmol. 1973;12(11):814–29.

Jeoung JW, Park KH. Comparison of Cirrus OCT and Stratus OCT on the ability to detect localized retinal nerve fiber layer defects in preperimetric glaucoma. Invest Ophthalmol Vis Sci. 2010;51(2):938–45.

Jeoung JW, Choi YJ, Park KH, Kim DM. Macular ganglion cell imaging study: glaucoma diagnostic accuracy of spectral-domain optical coherence tomography. Invest Ophthalmol Vis Sci. 2013;54(7):4422–9.

Jeoung JW, Kim TW, Weinreb RN, Kim SH, Park KH, Kim DM. Diagnostic ability of spectral-domain versus time-domain optical coherence tomography in preperimetric glaucoma. J Glaucoma. 2014;23(5):299–306.

Jonas JB, Dichtl A. Evaluation of the retinal nerve fiber layer. Surv Ophthalmol. 1996;40(5):369–78.

Jonas JB, Nguyen NX, Naumann GO. The retinal nerve fiber layer in normal eyes. Ophthalmology. 1989;96(5):627–32.

Kanamori A, Nakamura M, Escano MF, Seya R, Maeda H, Negi A. Evaluation of the glaucomatous damage on retinal nerve fiber layer thickness measured by optical coherence tomography. Am J Ophthalmol. 2003;135(4):513–20.

Kim DW, Jeoung JW, Kim YW, Girard MJ, Mari JM, Kim YK, et al. Prelamina and lamina cribrosa in glaucoma patients with unilateral visual field loss. Invest Ophthalmol Vis Sci. 2016a;57(4):1662–70.

Kim KE, Jeoung JW, Park KH, Kim DM, Kim SH. Diagnostic classification of macular ganglion cell and retinal nerve fiber layer analysis: differentiation of false-positives from glaucoma. Ophthalmology. 2015;122(3):502–10.

Kim YW, Jeoung JW, Kim DW, Girard MJ, Mari JM, Park KH, et al. Clinical assessment of lamina cribrosa curvature in eyes with primary open-angle glaucoma. PLoS One. 2016b;11(3):e0150260.

Langenegger SJ, Funk J, Töteberg-Harms M. Reproducibility of retinal nerve fiber layer thickness measurements using the eye tracker and the retest function of Spectralis SD-OCT in glaucomatous and healthy control eyes. Invest Ophthalmol Vis Sci. 2011;52(6):3338–44.

Lee WJ, Na KI, Kim YK, Jeoung JW, Park KH. Diagnostic ability of wide-field retinal nerve fiber layer maps using swept-source optical coherence tomography for detection of preperimetric and early perimetric glaucoma. J Glaucoma. 2017;26(6):577–85.

Lee WJ, Oh S, Kim YK, Jeoung JW, Park KH. Comparison of glaucoma-diagnostic ability between wide-field swept-source OCT retinal nerve fiber layer maps and spectral-domain OCT. Eye (Lond). 2018;32(9):1483–92.

Leite MT, Zangwill LM, Weinreb RN, Rao HL, Alencar LM, Sample PA, et al. Effect of disease severity on the performance of Cirrus spectral-domain OCT for glaucoma diagnosis. Invest Ophthalmol Vis Sci. 2010;51(8):4104–9.

Leite MT, Rao HL, Zangwill LM, Weinreb RN, Medeiros FA. Comparison of the diagnostic accuracies of the Spectralis, Cirrus, and RTVue optical coherence tomography devices in glaucoma. Ophthalmology. 2011;118(7):1334–9.

Leung CK, Cheung CY, Weinreb RN, Qiu Q, Liu S, Li H, et al. Retinal nerve fiber layer imaging with spectral-domain optical coherence tomography: a variability and diagnostic performance study. Ophthalmology. 2009;116(7):1257–63, 63.e1–2.

Leung CK, Yu M, Weinreb RN, Lai G, Xu G, Lam DS. Retinal nerve fiber layer imaging with spectral-domain optical coherence tomography: patterns of retinal nerve fiber layer progression. Ophthalmology. 2012;119(9):1858–66.

Mansouri K, Medeiros FA, Tatham AJ, Marchase N, Weinreb RN. Evaluation of retinal and choroidal thickness by swept-source optical coherence tomography: repeatability and assessment of artifacts. Am J Ophthalmol. 2014;157(5):1022–32.

Medeiros FA, Zangwill LM, Bowd C, Weinreb RN. Comparison of the GDx VCC scanning laser polarimeter, HRT II confocal scanning laser ophthalmoscope, and stratus OCT optical coherence tomograph for the detection of glaucoma. Arch Ophthalmol. 2004;122(6):827–37.

Mwanza JC, Durbin MK, Budenz DL, Sayyad FE, Chang RT, Neelakantan A, et al. Glaucoma diagnostic accuracy of ganglion cell-inner plexiform layer thickness: comparison with nerve fiber layer and optic nerve head. Ophthalmology. 2012;119(6):1151–8.

Radius RL, Anderson DR. The histology of retinal nerve fiber layer bundles and bundle defects. Arch Ophthalmol. 1979;97(5):948–50.

Sommer A, Miller NR, Pollack I, Maumenee AE, George T. The nerve fiber layer in the diagnosis of glaucoma. Arch Ophthalmol. 1977;95(12):2149–56.

Sommer A, Katz J, Quigley HA, Miller NR, Robin AL, Richter RC, et al. Clinically detectable nerve fiber atrophy precedes the onset of glaucomatous field loss. Arch Ophthalmol. 1991;109(1):77–83.

Vizzeri G, Weinreb RN, Gonzalez-Garcia AO, Bowd C, Medeiros FA, Sample PA, et al. Agreement between spectral-domain and time-domain OCT for measuring RNFL thickness. Br J Ophthalmol. 2009;93(6):775–81.